

# SAMPLE RATE OFFSET COMPENSATED ACOUSTIC ECHO CANCELLATION FOR MULTI-DEVICE SCENARIOS

Srikanth Korse, Oliver Thiergart, and Emanuël A. P. Habets

International Audio Laboratories Erlangen<sup>†</sup>, Am Wolfsmantel 33, 91058 Erlangen, Germany

## ABSTRACT

Acoustic echo cancellation (AEC) in multi-device scenarios is a challenging problem due to sample rate offset (SRO) between devices. The SRO hinders the convergence of the AEC filter, diminishing its performance. To address this, we approach the multi-device AEC scenario as a multi-channel AEC problem involving a multi-channel Kalman filter, SRO estimation, and resampling of far-end signals. Experiments in a two-device scenario show that our system mitigates the divergence of the multi-channel Kalman filter in the presence of SRO for both correlated and uncorrelated playback signals during echo-only and double-talk. Additionally, for devices with correlated playback signals, an independent single-channel AEC filter is crucial to ensure fast convergence of SRO estimation.

**Index Terms**— Acoustic Echo Cancellation, Kalman Filtering, Sample Rate Offset, Multi-Device

## 1. INTRODUCTION

Acoustic echo cancellation (AEC) is a critical acoustic signal processing technique employed to mitigate the echo caused by the acoustic coupling between loudspeakers and microphones [1–4]. In spatial teleconferencing systems [5] using multiple devices, as illustrated in Fig. 1, a primary device (such as a smartphone or a laptop) is typically hosts the conferencing application. The host is connected to multiple auxiliary loudspeakers via Bluetooth or WiFi. This setup is susceptible to sample rate offset (SRO), also known as clock drifts, due to the fact that each device operates on its own individual clock [6, 7]. The AEC algorithm running on the primary device must eliminate echoes originating from its own loudspeaker and those from the auxiliary loudspeakers in the presence of SRO. In the presence of SRO, the misalignment of the microphone and far-end signals degrades the AEC performance [8–12].

The degradation of AEC in the presence of SRO can be resolved through either asynchronous or synchronous methods. In asynchronous methods, the reference signals needed for AEC is estimated by using, for example, a set of fixed beamformers at different non-overlapping directions followed by an adaptive reference adaptation algorithm [11]. This approach avoids the explicit need for synchronization. However, this method encounters a significant issue of near-end speech distortion when the near-end speech is captured by the beamformer. Furthermore, it relies on the assumption that the near-end speech activity is sparse, which holds true for certain applications like keyword spotting but may not necessarily apply to teleconferencing scenarios.

In synchronous methods, the far-end signal is initially synchronized with the microphone signal before running the AEC. Pawig

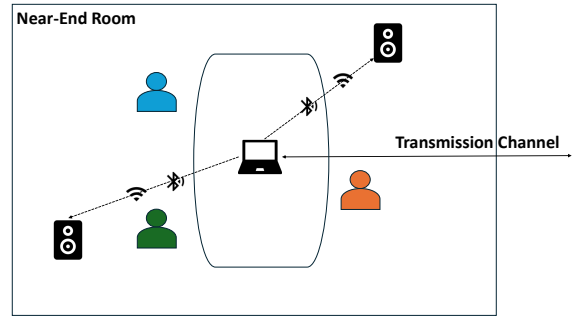


**Fig. 1:** Spatial teleconferencing system with the help of a main client connected to auxiliary devices via Bluetooth or WiFi.

et al. [9] modeled the SRO as a time scaling parameter. This parameter was then estimated and used for synchronizing the signals before applying the AEC. Abe et al. [10] estimated the SRO in the frequency domain using a simple extension of the least mean squares algorithm before rotating the phase of the far-end signal to approximate the time domain resampling. Helwani et al. [12] proposed a novel Kalman filtering approach which blindly accounts for the SRO. However, these studies are primarily limited to single-device scenarios, assuming an SRO between the microphone and loudspeaker due to mismatched sampling frequencies of the A/D and D/A converters.

In this study, we propose a synchronous method that addresses the two-device scenario as a two-channel AEC problem with SRO compensation. We assume that the primary device running the AEC has access to all far-end signals, but only before they are transmitted to the auxiliary loudspeakers. SRO compensation involves first estimating the SRO between the devices and then resampling the far-end signal using the estimated SRO before running the two-channel AEC. For SRO estimation, we use the robust dynamic weighted average coherence drift (DWACD) algorithm [13] belonging to the family of coherence drift methods [13–15]. We investigate the performance of both correlated and uncorrelated playback signals. Experiments in both echo-only and double-talk cases show that, for uncorrelated playback signals, it is possible to compensate for SRO. However, for correlated playback signals, there is a performance gap between the proposed method with both oracle and estimated SROs and the two-device AEC with no SRO. Finally, we show that an independent single-channel AEC filter is essential to ensure faster convergence of the estimated SRO.

## 2. MULTI-DEVICE SCENARIO

Let us consider a room with  $Q$  devices. Without loss of generality, we assume one microphone and one loudspeaker per device. The time-domain microphone signal of the primary device with index

<sup>†</sup>A joint institution of the Friedrich-Alexander-Universität Erlangen-Nürnberg (FAU) and Fraunhofer IIS, Germany.

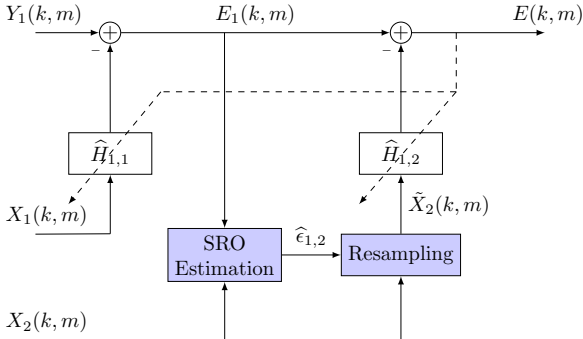


**Fig. 2:** Proposed two-device AEC envisioned as two-channel system with SRO compensation ("Variant 1").

$p \in \{1, Q\}$  is given by:

$$y_p \left[ \frac{n}{f_p} \right] = \sum_{q=0}^{Q-1} h_{p,q} \left[ \frac{n}{f_p} \right] * x_q \left[ \frac{n}{f_q} \right] + z_p \left[ \frac{n}{f_p} \right], \quad (1)$$

where  $*$  represents the convolution,  $n$  is the time index,  $x_q[n/f_q]$  is the far-end signal played from the loudspeaker of the  $q^{\text{th}}$  device,  $h_{p,q}[n/f_p]$  is the acoustic impulse response (AIR) between the loudspeaker of the  $q^{\text{th}}$  device and microphone of the  $p^{\text{th}}$  device,  $z_p[n/f_p]$  is the contribution of near-end talkers and noise at the microphone of the  $p^{\text{th}}$  device. The sampling rate of  $p^{\text{th}}$  and  $q^{\text{th}}$  device are given by  $f_p$  and  $f_q$ , respectively. The relation between  $f_p$  and  $f_q$  can be expressed in terms of SRO between the devices  $\epsilon_{p,q}$  as:

$$f_q = (1 + \epsilon_{p,q}) f_p, \quad (2)$$

where  $|\epsilon_{p,q}| \ll 1$  is usually expressed in parts-per-million (ppm).

This study considers a two-device scenario with the first device ( $p = 1$ ) as the primary device. We assume that i) there is no SRO between the loudspeaker and microphone of the primary device ( $\epsilon_{1,1} = 0$ ), and ii) there exists an unknown SRO  $\epsilon_{1,2}$  between the loudspeaker and microphone signals not belonging to the same device ( $|\epsilon_{1,2}| > 0$ ). With these assumptions, (1) becomes:

$$y_1 \left[ \frac{n}{f_1} \right] = h_{1,1}[n] * x_1 \left[ \frac{n}{f_1} \right] + h_{1,2}[n] * x_2 \left[ \frac{n}{f_2} \right] + z_1 \left[ \frac{n}{f_1} \right]. \quad (3)$$

Issues such as sampling time offset, variable SRO, and packet loss during transmission are beyond the scope of this paper. Since the primary device, on which the AEC is running, has no access to  $x_2 \left[ \frac{n}{f_2} \right]$  in (3), we express this signal in terms of the sampling rate  $f_1$  and SRO  $\epsilon_{1,2}$ . For this purpose, substituting (2) in (3), and applying Taylor series approximation to the term  $x_2 \left[ \frac{n}{(1+\epsilon_{1,2}) f_1} \right]$  [16], (3) can be approximated in frequency domain with sufficiently long window size  $N_w$  and hop size  $N_h$  as:

$$Y_1(k, m) = H_{1,1}(k, m) X_1(k, m) + Z_1(k, m) + H_{1,2}(k, m) \Lambda(k, m) X_2(k, m), \quad (4)$$

where  $\Lambda(k, m) = e^{\frac{-j2\pi k}{N_w} \left( \frac{mN_h \epsilon_{1,2}}{f_1} \right)}$ . In (4),  $X_1(k, m)$  and  $X_2(k, m)$  with frequency index  $k$  and frame index  $m$  are the frequency-domain representation of  $x_1 \left[ \frac{n}{f_1} \right]$  and  $x_2 \left[ \frac{n}{f_1} \right]$ , respectively.  $H_{p,q}(k, m)$  denotes the frequency-domain representation of  $h_{p,q}[n/f_p]$ . Note that (4) holds only if the condition  $\frac{mN_h \epsilon_{1,2}}{f_1} \ll N_w$  is satisfied [17].

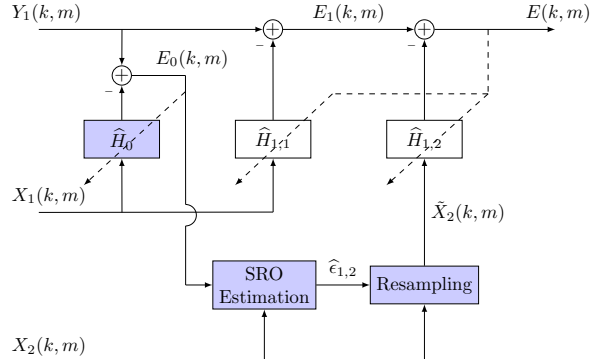


**Fig. 3:** Proposed two-device AEC envisioned as two-channel system with SRO compensation ("Variant 2").

The aim of two-device AEC running on the primary device is to eliminate the echoes from  $Y_1(k, m)$  by modeling the AIR  $H_{p,q}(k, m)$  with the help of a linear finite impulse response (FIR) filters. However, when  $X_2(k, m)$  is used as a reference signal, the linear FIR filter, which needs to model the AIR  $H_{1,2}(k, m) \Lambda(k, m)$ , does not converge sufficiently due to the time varying term  $\Lambda(k, m)$ . To mitigate the convergence issue, we need to compensate for the term  $\Lambda(k, m)$ .

### 3. PROPOSED METHOD

The two variants of the proposed two-device AEC envisioned as a two-channel AEC system with SRO compensation are shown in Figs. 2 and 3, respectively. The SRO compensation comprises of SRO estimation and resampling, which is described in Sec. 3.1. The two-channel AEC filter is described in detail in Sec. 3.2. The main difference between the two variants is the input signal used for SRO estimation. Variant 1 uses the error signal  $E_1$  as the input, while Variant 2 uses  $E_0$ . The error signal  $E_0$  is calculated by subtracting the estimated echo from the microphone signal, where the estimated echo is obtained from an independent single-channel AEC filter  $\hat{H}_0$ . For simplicity, in Sec. 3.1, we refer the input signal to SRO estimation as  $I(k, m)$ .

### 3.1. SRO compensation

To estimate the SRO, we use the DWACD algorithm proposed in [13]. Given the input signal  $I(k, m)$  and the reference signal  $X_2(k, m)$ , the SRO estimation relies on first computing the complex coherence function  $\Gamma(k, m)$ , which is given by:

$$\Gamma(k, m) = \frac{\Phi_{I X_2}(k, m)}{\sqrt{\Phi_{II}(k, m)\Phi_{X_2 X_2}(k, m)}}, \quad (5)$$

where  $\Phi_{I|X_2}$ ,  $\Phi_{II}$  and  $\Phi_{X_2|X_2}$  are the cross and auto power spectral densities, respectively. The phase function  $\tilde{P}(k, m)$  is then computed by the complex conjugated product of two consecutive complex coherence functions with a temporal distance of  $L$ . It is given by:

$$\tilde{P}(k, m) = \Gamma(k, m + L) \Gamma^*(k, m), \quad (6)$$

where  $*$  denotes the complex conjugate. The temporally averaged phase function  $P(k, m)$  and the generalized cross-correlation (GCC)  $p(\beta, m)$  are given by:

$$P(k, m) = \alpha P(k, m-1) + (1 - \alpha) \tilde{P}(k, m), \quad (7)$$

$$p(\beta, m) = \text{IDFT}\{P(k, m)\}, \quad (8)$$

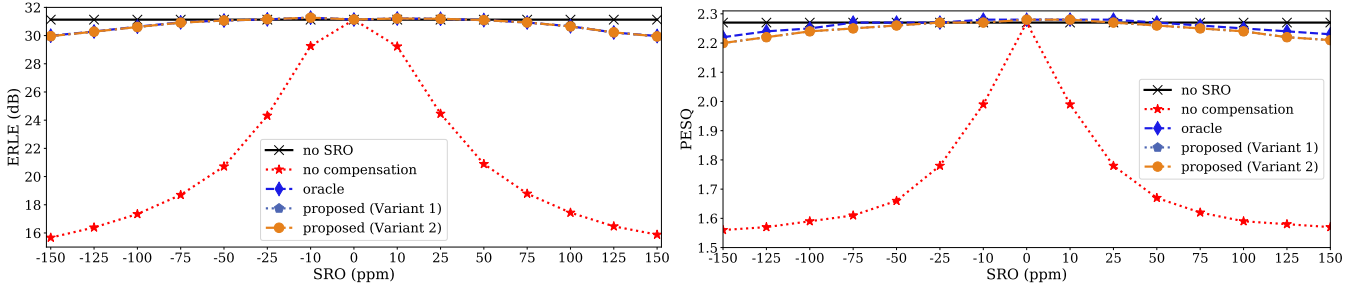


**Fig. 4:** Echo return loss enhancement (ERLE) (dB) vs. SRO (ppm) (left) and PESQ vs. SRO (ppm) (right) for uncorrelated playback signals.

where  $\alpha$  is the smoothing factor,  $\beta$  is the time-lag and IDFT is the inverse DFT. The estimated SRO  $\hat{\epsilon}_{1,2}$  is obtained by first finding the integer time-lag  $\beta_{\max}$  that maximizes the GCC:

$$\hat{\epsilon}_{1,2}(m) = -\frac{1}{L N_h} \beta_{\max} = -\frac{1}{L N_h} \arg \max_{\beta} |p(\beta, m)|. \quad (9)$$

Then, an accurate SRO estimate is obtained by determining the non-integer time-lag by performing a golden search in the interval given by  $[\beta_{\max} - 0.5, \beta_{\max} + 0.5]$ . The complex coherence function  $\Gamma(k, m)$  is estimated only when speech activity is detected in both the signals  $X_2(k, m)$  and  $I(k, m)$ . In this study, we used the energy-based ideal VAD to detect speech activity.

Once  $\hat{\epsilon}_{1,2}$  is estimated, we can compensate for the SRO. For this purpose, the term  $\Lambda(k, m)$  is computed using  $\hat{\epsilon}_{1,2}$ . Afterwards, we can obtain the resampled reference signal  $\tilde{X}_2(k, m) = X_2(k, m) \Lambda(k, m)$  to be used in the AEC. In addition, buffer management in both SRO estimation and resampling is essential to prevent the accumulation of sample drifts [13].

### 3.2. Two-channel AEC filter

The two-channel AEC filter is implemented as partitioned block frequency domain Kalman filter based on state-space architecture [4]. The filters and each partition within the filters are assumed to be mutually uncorrelated with zero mean. Under such assumption and the assumptions made by Kuech et al. in [4], the  $b^{\text{th}}$  partition of filter  $\hat{\mathbf{H}}_{p,q}$  and Kalman gain  $\mathbf{K}_{p,q}^b(m)$  is given by:

$$\hat{\mathbf{H}}_{p,q}^b(m+1) = A \left[ \hat{\mathbf{H}}_{p,q}^b(m) + \mathbf{K}_{p,q}^b(m) \mathbf{E}(m) \right], \quad (10)$$

$$\mathbf{K}_{p,q}^b(m) = \mathbf{P}_{p,q}^b(m) \left( \mathbf{X}_q^b \right)^H(m) \left[ \sum_{b=0}^{B-1} \mathbf{X}_q^b(m-1) \mathbf{P}_{p,q}^b(m) \left( \mathbf{X}_q^b \right)^H(m) + \frac{M}{V} \Psi_{ZZ}(m) \right]^{-1}, \quad (11)$$

where  $\hat{\mathbf{H}}_{p,q}^b(m) = \left[ \hat{H}_{p,q}^b(0, m), \hat{H}_{p,q}^b(1, m), \dots, \hat{H}_{p,q}^b(k, m) \right]^T$ ,  $A$  is the transition factor,  $T$  is the transpose,  $\mathbf{E}(m)$  is the error signal, superscript  $H$  denotes the conjugate transpose of a matrix,  $\Psi_{ZZ}(m)$  is the covariance of the near-end spectrum  $Z(m)$ ,  $\mathbf{X}_q^b$  is the  $q^{\text{th}}$  far-end signal,  $M$  and  $V$  are the hop size and frame length respectively. The covariance matrix of the coefficient error vector  $\mathbf{P}_{p,q}^b(m)$  is given by:

$$\mathbf{P}_{p,q}^b(m) = A^2 \left[ \mathbf{I}_M - \mathbf{K}_{p,q}^b(m-1) \mathbf{X}_q^b(m-1) \right] \mathbf{P}_{p,q}^b(m-1) + \Psi_{b,\Delta\Delta}(m), \quad (12)$$

where  $\Psi_{b,\Delta\Delta}$  is the covariance of the temporal variations of the acoustic transfer path. To ensure the convergence of the linear FIR filter  $\hat{\mathbf{H}}_{1,2}^b$ , we use  $\tilde{X}_2(k, m)$  instead  $X_2(k, m)$  of as the reference signal.

## 4. EXPERIMENTAL RESULTS

The performance of our proposed system is evaluated under both correlated cases, where the devices are playing back the same signal, and uncorrelated cases, where the devices are playing back different signals. In the echo-only scenario, echo return loss enhancement (ERLE) [1] is used to evaluate the performance whereas, perceptual evaluation of speech quality (PESQ) [18] is used to assess the performance in the double-talk scenario by comparing the output of the proposed system with that of ground-truth near-end speech. For the evaluation, the above-mentioned metrics were computed by averaging the result over 50 test files.

### 4.1. Test signal generation

To generate the microphone signals, we first created far-end and near-end signals of duration 36 s at a sampling rate of 16 kHz from the training set *si\_tr\_s* of WSJ0 database [19]. These files were normalized to -25 dBFS before convolving with simulated room impulse responses (RIRs) [20]. The size of the room was chosen randomly with a uniform distribution between [5,5,3] m and [8,8,6] m. The reverberation time was set to a random value between 0.2 s and 0.5 s with uniform probability. The device positions and near-end talker positions were randomly chosen within the room. However, it was ensured that they were at least 0.75 m away from the walls. Constant SROs in the range of  $\pm 150$  ppm [21] were simulated on the echo signals using the STFT method proposed in [22] using segment length of 8192 samples [13]. All the SRO simulated echo signals were added along with near-end speech, if present, before adding a Gaussian noise at 40 dB SNR to simulate sensor noise.

### 4.2. Evaluation

We compare the two variants of our system (Variant 1 and Variant 2) against systems assuming no SRO between the devices (no SRO), no SRO compensation (no compensation), and oracle SRO compensation (oracle)<sup>1</sup>. For the echo-only scenario, ERLE is computed using the last 30 s, whereas, for the double-talk scenario, PESQ is calculated using the entire signal. For the estimation of the SRO, two previous segments, each of length 8192 samples corresponding to 0.512 s, are used. Hence, the estimation of the SRO does not add any additional delay. The power spectral densities are computed by the Welch method with a hop length of 512 samples (32 ms), and the smoothing parameter  $\alpha$  is set to 0.95. The Kalman filters are implemented with 10 taps, an FFT length of 512 samples, and a hop length

<sup>1</sup><https://www.audiolabs-erlangen.de/resources/>  
2024-IWAENC-SRO-MDAEC

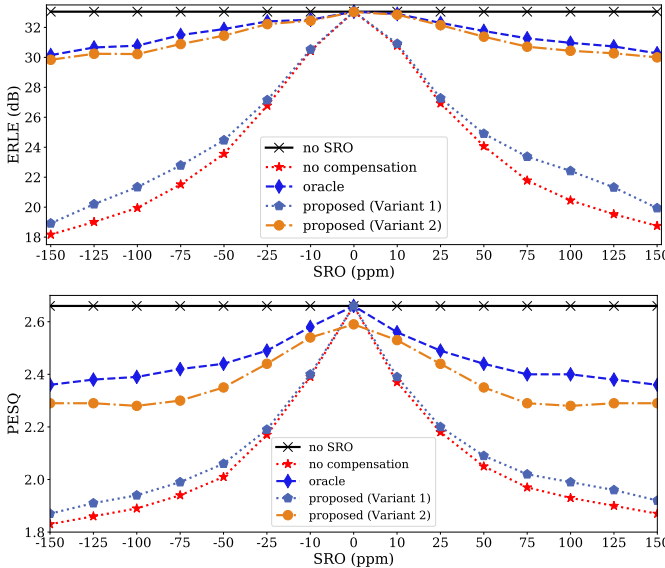
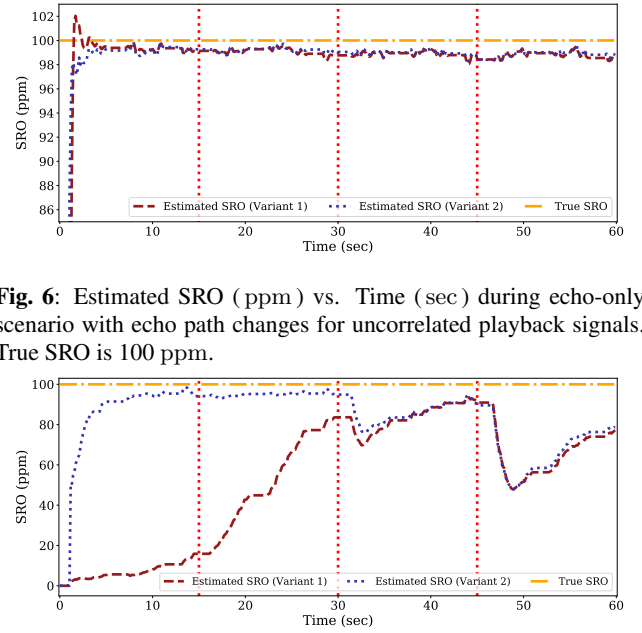


**Fig. 5:** Top: ERLE(dB) vs. SRO(ppm), Bottom: PESQ vs. SRO (ppm) for correlated playback signals.

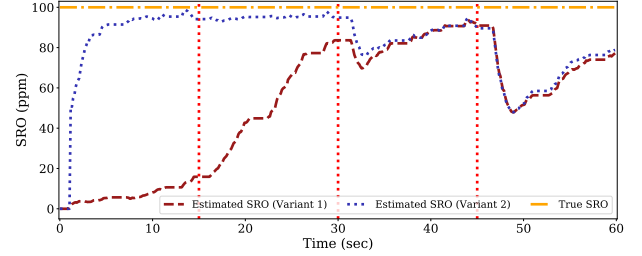
of 256 samples, which corresponds to a filter length of 160 ms in the time domain. The transition parameter (A) is set to 0.999 [4].

Figure 4 evaluates the performance of the compared systems for echo-only and double-talk scenarios for uncorrelated playback signals. When the SRO is uncompensated, the performance of the system drops since AEC filter  $\hat{H}_{1,2}$  fails to converge to the true AIR  $H_{1,2}$ . When compensated for the SRO, both the variants of the proposed system reach the performance of the system that assumes no SRO between the devices, especially at SRO values smaller than  $\pm 75$  ppm. In addition, the performance of these variants matches that of the oracle system. The performance in the double-talk scenario is similar to the echo-only scenario except for a minor gap with the system that uses oracle SRO, especially at higher SRO values.

Figure 5 evaluates the performance of the compared systems for echo-only and double-talk scenarios for correlated playback signals. When the SRO is uncompensated, the system's performance drops due to the divergence of the two-channel AEC. In Variant 1 of the proposed system, the filter convergence and SRO estimation impact each other, leading to slow convergence of SRO. Hence, the performance of Variant 1 is similar to that of the system with no compensation in both echo-only and double-talk scenarios. Hence, in Variant 2 of the proposed system, an independent single-channel AEC filter  $\hat{H}_0$  is employed to decouple the filter convergence and SRO estimation. This decoupling helps the estimated SRO to converge faster to the true SRO. In the echo-only scenario, the performance of Variant 2 of the proposed system and the system using oracle SRO has almost identical performance. However, in the double-talk scenario, the performance of variant 2 of the proposed system fails to match the system's performance using oracle SRO. The main reason for this is the inaccuracies in the estimated SRO since the SRO estimation in the double-talk scenario is not as robust as in the echo-only scenario. Variant 2 of the proposed system and the oracle system fail to compensate for the effect of SRO. This is because, although the SRO introduces some decorrelation, the filter  $\hat{H}_{1,1}$  and  $\hat{H}_{1,2}$  do not converge to the true AIR  $H_{1,1}$  and  $H_{2,2}$  respectively.



**Fig. 6:** Estimated SRO (ppm) vs. Time (sec) during echo-only scenario with echo path changes for uncorrelated playback signals. True SRO is 100 ppm.



**Fig. 7:** Estimated SRO (ppm) vs. Time (sec) during echo-only scenario with echo path changes for correlated playback signals. True SRO is 100 ppm.

#### 4.3. SRO estimation in the presence of echo path change

In this section, we evaluate the robustness of SRO estimation in echo-only scenarios for uncorrelated and correlated playback signals. We simulate three echo path changes on a signal with duration 60 s. At 15 s, only the position of device two is changed, thus affecting the AIR  $H_{1,2}$ . At 30 s, only the microphone of device one is changed, affecting the AIR  $H_{1,1}$ . At 45 s, both the microphone of device one and device two are simultaneously changed, affecting the AIR  $H_{1,2}$  and  $H_{1,1}$  simultaneously.

Figure 6 compares the estimated SRO for the two variants of the proposed system with the true SRO for uncorrelated playback signals. The estimated SRO for both the variants quickly converges to the true SRO and is robust to all the simulated echo path changes.

Figure 7 compares the estimated SRO for the two variants of the proposed system with the true SRO for correlated playback signals. The SRO estimation converges to true SRO faster in Variant 2 when compared to Variant 1. Once the SRO estimation converges, SRO estimation of both system variants performs similarly. In addition, we can observe that change in AIR  $H_{1,2}$  has no impact on the SRO estimation, whereas change in AIR  $H_{1,1}$  leads to a small drop in the estimated SRO. However, a simultaneous change in AIR  $H_{1,2}$  and  $H_{1,1}$  simultaneously shows a huge drop in the estimated SRO.

## 5. CONCLUSION

We proposed two variants of two-channel AEC for addressing the two-device AEC problem in the presence of SRO and evaluated them for both uncorrelated or correlated playback signals in echo-only and double-talk scenarios. We showed that for uncorrelated playback signals, it is possible to compensate for SRO and reach the performance of the system with no SRO. Additionally, we demonstrated that the SRO estimation is robust to echo path changes. For the correlated playback signals, to ensure faster convergence of SRO, we use an independent single-channel AEC filter. This is primarily done to decouple the filter convergence from the SRO estimation.

## 6. REFERENCES

[1] E. Hansler and G. Schmidt, *Acoustic Echo and Noise Control: A Practical Approach*, Wiley-Interscience, USA, 2004.

[2] G. Enzner and P. Vary, “Frequency-domain adaptive Kalman filter for acoustic echo control in hands-free telephones,” *Signal Processing*, vol. 86, no. 6, pp. 1140–1156, June 2006.

[3] S. Malik and G. Enzner, “Recursive Bayesian Control of Multi-channel Acoustic Echo Cancellation,” *IEEE Signal Processing Letters*, vol. 18, no. 11, pp. 619–622, Nov. 2011.

[4] F. Kuech, E. Mabande, and G. Enzner, “State-space architecture of the partitioned-block-based acoustic echo controller,” in *IEEE International Conference on Acoustics, Speech and Signal Processing (ICASSP)*, Florence, Italy, May 2014, pp. 1295–1299, IEEE.

[5] J. Herre, C. Falch, D. Mahane, G. Del Galdo, M. Kallinger, and O. Thiergart, “Interactive teleconferencing combining spatial audio object coding and dirac technology,” *J. Audio Eng. Soc.*, vol. 59, no. 12, pp. 924–935, 2012.

[6] M. Guggenberger, M. Lux, and L. Böszörmenyi, “Clock-Drift: a mobile application for measuring drift in multimedia devices,” in *Proceedings of the 22nd ACM international conference on Multimedia*, Orlando Florida USA, Nov. 2014, pp. 767–768, ACM.

[7] M. Guggenberger, M. Lux, and L. Böszörmenyi, “An Analysis of Time Drift in Hand-Held Recording Devices,” in *MultiMedia Modeling*, vol. 8935, pp. 203–213. Springer International Publishing, Cham, 2015, Series Title: Lecture Notes in Computer Science.

[8] E. Robledo-Arnuncio, T. S. Wada, and B-H. Juang, “On Dealing with Sampling Rate Mismatches in Blind Source Separation and Acoustic Echo Cancellation,” in *IEEE Workshop on Applications of Signal Processing to Audio and Acoustics*, New Paltz, NY, USA, Oct. 2007, pp. 34–37, IEEE.

[9] M. Pawig, G. Enzner, and P. Vary, “Adaptive Sampling Rate Correction for Acoustic Echo Control in Voice-Over-IP,” *IEEE Transactions on Signal Processing*, vol. 58, no. 1, pp. 189–199, Jan. 2010.

[10] M. Abe and M. Nishiguchi, “Frequency domain acoustic echo canceller that handles asynchronous A/D and D/A clocks,” in *IEEE International Conference on Acoustics, Speech and Signal Processing (ICASSP)*, Florence, Italy, May 2014, pp. 5924–5928, IEEE.

[11] R. Ayrapetian, P. Hilmes, M. Mansour, T. Kristjansson, and C. Murgia, “Asynchronous Acoustic Echo Cancellation Over Wireless Channels,” in *IEEE International Conference on Acoustics, Speech and Signal Processing (ICASSP)*, Toronto, ON, Canada, June 2021, pp. 116–120, IEEE.

[12] K. Helwani, E. Soltanmohammadi, M. M Goodwin, and A. Krishnaswamy, “Clock Skew Robust Acoustic Echo Cancellation,” in *Interspeech 2022*, Sept. 2022, pp. 2533–2537, ISCA.

[13] T. Gburrek, J. Schmalenstroer, and R. Haeb-Umbach, “On Synchronization of Wireless Acoustic Sensor Networks in the Presence of Time-Varying Sampling Rate Offsets and Speaker Changes,” in *IEEE International Conference on Acoustics, Speech and Signal Processing (ICASSP)*, Singapore, Singapore, May 2022, pp. 916–920, IEEE.

[14] J. Schmalenstroer, J. Heymann, L. Drude, C. Boeddecker, and R. Haeb-Umbach, “Multi-stage coherence drift based sampling rate synchronization for acoustic beamforming,” in *IEEE 19th International Workshop on Multimedia Signal Processing (MMSP)*, Luton, Oct. 2017, pp. 1–6, IEEE.

[15] A. Chinaev, G. Enzner, T. Gburrek, and J. Schmalenstroer, “Online Estimation of Sampling Rate Offsets in Wireless Acoustic Sensor Networks with Packet Loss,” in *29th European Signal Processing Conference (EUSIPCO)*, Dublin, Ireland, Aug. 2021, pp. 1110–1114, IEEE.

[16] S. Markovich-Golan, S. Gannot, and I. Cohen, “Blind sampling rate offset estimation and compensation in wireless acoustic sensor networks with application to beamforming,” in *International Workshop on Acoustic Signal Enhancement*, 2012, pp. 1–4.

[17] L. Wang and S. Doclo, “Correlation maximization-based sampling rate offset estimation for distributed microphone arrays,” *IEEE/ACM Transactions on Audio, Speech, and Language Processing*, vol. 24, no. 3, pp. 571–582, 2016.

[18] ITU-T, “P.862: Perceptual evaluation of speech quality (pesq): An objective method for end-to-end speech quality assessment of narrow-band telephone networks and speech codecs,” 2001.

[19] Y. Z. Isik, J. Le Roux, Z. Chen, S. Watanabe, and J. R. Hershey, “Single-channel multi-speaker separation using deep clustering,” *CoRR*, vol. abs/1607.02173, 2016.

[20] Emanuël A. P. Habets, “Room impulse response (RIR) generator,” 2008.

[21] J. Schmalenstroer, T. Gburrek, and R. Haeb-Umbach, “LibriWASN: A data set for meeting separation, diarization, and recognition with asynchronous recording devices,” in *ITG conference on Speech Communication (ITG 2023)*, Sep 2023.

[22] J. Schmalenstroer and R. Haeb-Umbach, “Efficient sampling rate offset compensation - an overlap-save based approach,” in *26th European Signal Processing Conference (EUSIPCO)*, 2018, pp. 499–503.